ZEUS-prel-06-009

Submitted to the
XXXIII International Conference on High Energy Physics
July 26 - August 2, 2006, Moscow, Russia

Abstract: -

Session: QCD hard interactions
Electroweak

Three and four-jet final states in photoproduction at HERA

ZEUS Collaboration

Abstract

Three- and four-jet final states have been measured in photoproduction at HERA using the ZEUS detector and an integrated luminosity of 121 pb^{-1}. The three-jet results are presented in a wider phase-space and are based on over seven times the luminosity of the previous HERA publication. The four-jet photoproduction cross section has been measured for the first time and represents the highest order processes studied at HERA. The events have been studied in a semi-inclusive, $M_{nj} \geq 25$ GeV, and a high-mass region, $M_{nj} \geq 50$ GeV, where M_{nj} is the invariant mass of the n-jet system. The three-jet cross sections have been compared to an $\mathcal{O}(\alpha\alpha_s^2)$ perturbative QCD calculation. The calculation describes the higher-mass region reasonably well but underestimates the data for $M_{3\mathrm{j}} < 50$ GeV. In addition, the three- and four-jet cross sections have been compared with two leading-logarithm parton-shower Monte Carlo models, with and without multi-parton interactions.

1 Introduction

In photoproduction, a quasi-real photon, emitted by the incoming positron, interacts with a parton from the proton. Photoproduction may be categorised at leading order (LO) as being either direct, if the photon interacts as a point-like particle, or resolved, if it fluctuates into a partonic system, and subsequently transfers only a fraction of its momentum to the hard interaction. At higher-orders this distinction is blurred.

Multi-jet events are of particular interest as they are manifestly produced by processes of high order in the strong coupling constant, α_s. Perturbative quantum chromodynamics (pQCD) calculations for multi-jets in photoproduction are only available at $\mathcal{O}(\alpha\alpha_s^2)$, where α is the fine structure constant.

Multi-parton interactions (MPIs) can occur at HERA in resolved photoproduction. In MPI models, more than one pair of partons from the incoming hadrons may interact. A schematic of an MPI event is shown in Fig. 1. The secondary scatters generate additional hadronic energy flow in the event, the topology of which is poorly understood theoretically.

Three-jet photoproduction events have been studied before at HERA in a high-mass region given by $M_{3j} \geq 50$ GeV [1]. Multi-jet final states have also been studied in deep inelastic scattering (DIS) at HERA [2–5].

In this paper, differential cross sections are presented for three-jet photoproduction in a wider M_{3j} region, based on over seven times the luminosity of the previous HERA publications. The four-jet photoproduction cross sections are presented here for the first time. The three-jet cross sections have been compared with an $\mathcal{O}(\alpha\alpha_s^2)$ pQCD calculation. Both the three- and four-jet cross sections are compared to the predictions of (LO matrix element plus parton showers) Monte Carlo (MC) models, both with and without MPIs.

2 Variable definitions

The invariant mass of the n-jet system, M_{nj}, is defined as follows,

$$M_{\mathrm{nj}} = \sqrt{\left(\sum_{\mathrm{i=1}}^{\mathrm{n}} p_i^\mu\right)^2}, \tag{1}$$

where p_i^μ is the four-vector of the i^{th} jet.

The fraction of the photon's momentum that is exchanged in the interaction, x_γ, is approximated using the observable x_γ^{obs},

$$x_\gamma^{\rm obs} = \frac{\sum_{\rm i=1}^{\rm n} E_{\rm T,i}^{\rm jet} \exp(-\eta_i^{\rm jet})}{2yE_e}, \tag{2}$$

where $E_{\rm T,i}^{\rm jet}$ and $\eta_i^{\rm jet}$ are the transverse energy and pseudorapidity of the $i^{\rm th}$ jet, respectively, y is the fraction of the initial electron's momentum that was given to the quasi-real photon and $E_e = 27.5$ GeV denotes the energy of the incoming electron.

For the multi-jet variables, $\cos(\theta_3^{(\prime)})$, $\cos(\psi_3^{(\prime)})$ and $X_3^{(\prime)}$, defined below, the three (four) jets in the final state were boosted to the multi-jet centre-of-mass frame and ordered by decreasing energy: $E_3 \geq E_4 \geq E_5 (\geq E_6)$.

In four-jet events the two jets with lowest M_{2j} have been combined and the events are treated as a three-jet sample.

Angular variables are defined as:

$$\cos(\theta_{3^{(\prime)}}) = \frac{\boldsymbol{p}_{\rm beam} \cdot \boldsymbol{p}_{3^{(\prime)}}}{|\boldsymbol{p}_{\rm beam}||\boldsymbol{p}_{3^{(\prime)}}|}, \tag{3}$$

$$\cos(\psi_{3^{(\prime)}}) = \frac{(\boldsymbol{p}_{\rm beam} \times \boldsymbol{p}_{3^{(\prime)}}) \cdot (\boldsymbol{p}_{4^{(\prime)}} \times \boldsymbol{p}_{5^{(\prime)}})}{|\boldsymbol{p}_{\rm beam} \times \boldsymbol{p}_{3^{(\prime)}}||\boldsymbol{p}_{4^{(\prime)}} \times \boldsymbol{p}_{5^{(\prime)}}|}. \tag{4}$$

The energy distribution of the three-jet system is described via energy sharing variables, one of which is $X_{3^{(\prime)}}$,

$$X_{3^{(\prime)}} = \frac{2E_{3^{(\prime)}}}{E_{3^{(\prime)}} + E_{4^{(\prime)}} + E_{5^{(\prime)}}}, \tag{5}$$

3 Event reconstruction and selection

The data were collected using the ZEUS detector during the 1996 to 2000 running periods. In 1996 and 1997, HERA collided positrons with protons, with energies of $E_e = 27.5$ GeV and $E_p = 820$ GeV, respectively. From 1998 onwards the proton beam energy was raised to $E_p = 920$ GeV. A subsample of the 1998 data is comprised of electron-proton collisions[1]. The total sample corresponds to an integrated luminosity of $121 \pm 2\%$ pb^{-1}. A detailed description of the ZEUS detector can be found elsewhere [6, 7].

A three-level trigger system was used to select events online [7, 8]. At the third level, jets were reconstructed by applying a jet algorithm to the ZEUS calorimeter (CAL) cells. Events with at least two jets, with $E_T^{\rm jet} \geq 4$ GeV and $\eta^{\rm jet} \leq 2.5$, were accepted.

[1] From now on the word "electron" is used as a generic term for electrons and positrons.

In the offline analysis, the hadronic final state was reconstructed using energy flow objects [9, 10] (EFOs), which are formed from a combination of track and calorimeter information. The EFOs are corrected [11] to account for energy losses in the dead material and were defined to be massless.

The data sample was selected by requiring that,

- the longitudinal position of the reconstructed vertex was in the range $|Z_{\rm vtx}| \leq 40$ cm, to select events consistent with an *ep* collision;
- $y_{\rm JB} \geq 0.2$, to remove beam gas events;
- no scattered electron was observed in the CAL with $y_e \geq 0.85$, to remove background from DIS, where $y_e = 1 - \frac{E_{e'}}{2E_e}\cos(1-\theta_{e'})$;
- $y_{\rm JB} \leq 0.85$, to remove remaining contamination from DIS;
- $P_T^{\rm miss}/\sqrt{E_T} \leq 2$ GeV$^{1/2}$, where $P_T^{\rm miss}$ is the missing transverse momentum and E_T is the total transverse energy, to remove background from charged current events.

The energy and angular reconstruction of the jets, formed from the energy corrected EFOs, exhibited no systematic bias with respect to that at the hadron-level and thus the jet and phase-space requirements made at the detector-level reflected those defining the hadron-level measurement, namely,

- three or four jets with $|\eta^{\rm jet}| \leq 2.4$ such that two possessed an $E_T^{\rm jet} \geq 7$ GeV and the rest, an $E_T^{\rm jet} \geq 5$ GeV;
- $\cos(\theta_{3(\prime)}) \leq 0.95$;
- $X_{3(\prime)} \leq 0.95$.

After all of the cuts had been applied, the semi-inclusive- and high-mass, three-jet data samples had 426413 and 39448 events, respectively, and the semi-inclusive- and high-mass, four-jet samples had 84059 and 18597 events.

4 Definition of the cross section

Photoproduction events were studied in a kinematic region given by $Q^2 < 1$ GeV^2, where Q^2 is the virtuality of the exchanged boson, and with a photon-proton centre-of-mass energy, $W_{\gamma\rm p}$, in the range 142 to 293 GeV. Each event was required to have at least three or four jets with $|\eta^{\rm jet}| \leq 2.4$, such that the two highest $E_T^{\rm jet}$ jets had $E_T^{\rm jet} \geq 7$ GeV and any additional jets had $E_T^{\rm jet} \geq 5$ GeV. The jets were reconstructed by applying the k_T cluster algorithm [12] in the longitudinally invariant inclusive mode [13] to the final-state hadrons. The jets were defined to be massless. In addition, it was required that $\cos(\theta_{3(\prime)}) \leq 0.95$

and $X_{3(')} \leq 0.95$ to remove regions of phase-space heavily depleted by the $E_T^{\rm jet}$ and $\eta^{\rm jet}$ selection criteria. In both the three- and four-jet analyses, two mass regions were studied. The first will be referred to as the semi-inclusive-mass region and has $M_{\rm nj} \geq 25$ GeV and the second, the high-mass region, with $M_{\rm nj} \geq 50$ GeV.

5 Monte Carlo models

Two MC generators were used to simulate photoproduction events, namely, HERWIG version 6.505 [14] and PYTHIA 6.146 and 6.206 [15]. Both models include the LO ($2 \rightarrow 2$) matrix elements, approximate higher-order processes using initial state radiation (ISR) and final state radiation (FSR) parton-showers and simulate hadronisation. Direct and resolved photoproduction samples were generated separately. The implementation of the parton-showers and hadronisation models differ in both generators. PYTHIA parton-showers are parameterised using m_a^2, the mass of the branching parton squared. The angular ordering of the subsequent emissions, resulting from colour coherence, is enforced as an additional constraint [15]. In contrast, parton-showers in HERWIG are ordered via emission angle and so this coherence effect is intrinsically present [16–18]. Hadronisation in HERWIG is simulated using the cluster model [19] while PYTHIA uses the Lund string model [20, 21].

5.1 Underlying-event models

In the HERWIG 6.505 samples, MPIs were simulated using a separate program called JIMMY 4.0 [22–25]. It is a simple eikonal model that approximates the interacting hadrons as disks that are extended in the transverse plane. An impact parameter, b, quantifies the degree to which the two disks overlap during the collision.

The PYTHIA underlying-event model that was used is known as the simple model [15]. It estimates the average number of MPIs per event, $\bar{n}$, as, $\bar{n} = \sigma_H(p_{\rm T,min})/\sigma_{\rm ND}(s)$, where σ_H and $\sigma_{\rm ND}$ are the inclusive-hard and non-diffractive, inelastic cross sections, respectively. The number of MPIs is assumed to obey a Poisson distribution. The probability that the secondary collisions occur with transverse momentum p_T is given by $P(p_T) = (1/\sigma_{\rm ND}(s))({\rm d}\sigma_H/{\rm d}p_T)$. The simple model proceeds by ordering the secondary interactions in terms of p_T, and then calculating the probability of each successive scatter.

5.2 Monte Carlo samples

The Monte Carlo simulations were used for two purposes: to correct the data for detector effects, and to compare to the measured hadron-level cross sections. The samples used to correct the data included a full GEANT 3.13 [26] simulation of the ZEUS detector and three-level trigger. The resolved and direct contributions were combined in the ratio that gave the best fit to the $x_\gamma^{\rm obs}$ distribution in the data. The resolved and direct samples used to compare to the hadron-level cross sections, however, were combined in the ratio predicted by the MC models.

Each of the HERWIG samples were generated with the minimum p_T of the $(2 \rightarrow 2)$ partonic collision, $\hat{p}_T^{\rm min}$, set to 2 GeV and using the CTEQ5L [27] and GRV-G LO [28] parameterisations for the proton and photon structure functions, respectively. MPIs were simulated using JIMMY 4.0, with the minimum p_T of the secondary scatters, $\hat{p}_T^{\rm mpi}$, set to 1.8 GeV. In addition, the probability that the photon would resolve via a large hadronic-like fluctuation, $P_{\rm res}$, was changed from $P_{\rm res} = 1/300$ to $P_{\rm res} = 1/150$. Finally, the effective transverse radius of the proton squared, was increased by a factor of 2.5 from its default. These alterations were the result of a simultaneous tune to three- and four-jet γp cross sections measured in this analysis double differentially in $x_\gamma^{\rm obs}$ and $M_{\rm nj}$, in a phase-space region similar to that studied here [29].

The PYTHIA 6.146 sample was generated with $\hat{p}_T^{\rm min} = 3$ GeV using the GRV 94 LO [30] and WHIT-G 2 [31] parameterisations for the proton and photon structure functions, respectively. Multi-parton interactions were simulated using the simple model with $\hat{p}_T^{\rm mpi} =$ 2 GeV. The PYTHIA 6.206 samples that were compared to the hadron-level cross sections, were generated with $\hat{p}_T^{\rm min} = 2$ GeV, $\hat{p}_T^{\rm mpi} = 1.5$ GeV and used the CTEQ5L and GRV-G LO parameterisations for the proton and photon structure functions, respectively. This combination of $\hat{p}_T^{\rm min}$ and $\hat{p}_T^{\rm mpi}$ came from a tune to generic collider data, from HERA, LEP and the Tevatron [32]. This will be referred to as the PYTHIA "generic tune".

Both MC simulations underestimated the magnitude of the cross sections. To better compare the shape of the differential cross sections the MC predictions were scaled. The magnitude of the scaling factor was calculated as the ratio of the measured cross section above $M_{nj} \geq 70$ GeV, where MPIs are expected to be negligible, divided by that predicted by each MC model without MPIs. The scaling factors applied to the HERWIG and PYTHIA three-jet (four-jet) predictions were 1.8 (2.4) and 4.0 (7.4), respectively.

6 The $\mathcal{O}(\alpha\alpha_s^2)$ pQCD calculation

The three-jet differential cross sections were compared with a $\mathcal{O}(\alpha\alpha_s^2)$ pQCD calculation by Klasen, Kleinwort and Kramer [33, 34]. The calculation is LO for this process. The calculation was corrected for hadronisation and MPI effects. These were obtained using the HERWIG and PYTHIA samples. The hadronisation corrections, $\mathcal{C}_{\rm had}$, were calculated by taking the bin-by-bin ratio of the MC cross sections at the hadron- and parton-shower-levels, $\mathcal{C}_{\rm had} = \sigma_{\rm HL}/\sigma_{\rm PSL}$. To obtain $\sigma_{\rm PSL}$, the k_T cluster algorithm was run over all of the partons after the parton-shower, prior to hadronisation. The hadronisation corrections were found to cause a negative effect of $\mathcal{O}(20\%)$ on the cross section. The MPI corrections, $\mathcal{C}_{\rm MPI}$, were calculated by taking the bin-by-bin ratio of the HERWIG hadron-level cross sections, with and without MPIs, $\mathcal{C}_{\rm MPI} = \sigma_{\rm HL}^{\rm MPI}/\sigma_{\rm HL}^{\rm noMPI}$. The MPI corrections were $\mathcal{O}(25\%)$ in the semi-inclusive-mass region but small ($< 5\%$) in the MPI insensitive, high-mass sample. The PYTHIA MC was not used to estimate $\mathcal{C}_{\rm MPI}$ since its treatment of MPIs did not describe the data.

The $E_T^{\rm jet}$ of the hardest jet, $E_T^{\rm max}$, was chosen for both the renormalisation and factorisation scales, μ. The theoretical scale uncertainty was evaluated by varying μ, setting it to $2^{\pm 1}E_T^{\rm max}$. The value of the strong coupling constant, α_s, was calculated with one loop precision and assuming five active flavours. A value of $\Lambda_{\overline{\rm MS}}^{(5)} = 181$ MeV was taken. The CTEQ4L [35] proton and GRV-G LO [36] photon PDFs were used for the calculation.

7 Acceptance corrections

Detector effects and trigger inefficiencies were corrected using an unfolding matrix [29]. Typical corrections applied to the semi-inclusive- and high-mass three-jet data were $\sim 20\%$ and $\sim 25\%$, respectively. Those applied to the semi-inclusive- and high-mass four-jet data were $\sim 45\%$ and $\sim 15\%$, respectively.

The measured cross sections, $\sigma_{\sqrt{\rm s}}$, at $\sqrt{s} = 300$ GeV and $\sqrt{s} = 318$ GeV were combined using the following formula,

$$\sigma_{318}^{\rm comb} = \frac{\sigma_{300} \cdot (\sigma_{318}^{\rm mc}/\sigma_{300}^{\rm mc}) \cdot \mathcal{L}_{300} + \sigma_{318} \cdot \mathcal{L}_{318}}{\mathcal{L}_{300} + \mathcal{L}_{318}}, \qquad (6)$$

where $\mathcal{L}_{\sqrt{\rm s}}$ is the luminosity and $\sigma_{\sqrt{\rm s}}^{\rm mc}$ is the predicted MC cross section. The ratio $\sigma_{318}^{\rm mc}/\sigma_{300}^{\rm mc}$ was obtained using HERWIG. The ratio was ~ 1.1 for all but the semi-inclusive-mass four-jet sample, where it was slightly larger.

8 Systematic Uncertainties

A detailed study of the sources of systematic uncertainty associated with the measurement was performed [29]. Only the most significant sources are listed here:

- the energy scale uncertainty was estimated to be $\pm 3\%$ in the forward, $\pm 1\%$ in the barrel and $\pm 2\%$ in the rear sections of the CAL. This typically leads to a systematic uncertainty of $\sim \pm 7\%$ and $\sim \pm 8\%$ in the semi-inclusive- and high-mass three-jet differential cross sections, and $\sim \pm 10\%$ and $\sim \pm 10\%$ in the semi-inclusive- and high-mass four-jet differential cross sections;
- using PYTHIA instead of HERWIG to determine the unfolding matrix determined a systematic effect that was typically $\sim -9\%$ and $\sim +7\%$ in the semi-inclusive- and high-mass three-jet differential cross sections, and $\sim -6\%$ and $\sim +11\%$ in the semi-inclusive- and high-mass four-jet differential cross sections;
- the offline selection criteria were varied up and down by the detector resolution. The largest effect was associated with the $E_T^{\rm jet}$ resolution. The typical uncertainty was $\sim \pm 4\%$ and $\sim \pm 1\%$ in the semi-inclusive- and high-mass three-jet differential cross sections, and $\sim \pm 10\%$ and $\sim \pm 4\%$ in the semi-inclusive- and high-mass four-jet differential cross sections.

These systematic uncertainties were added in quadrature. The average systematic uncertainty, not including that associated with the calorimeter energy scale uncertainty, for the four samples is as follows. In the three-jet semi-inclusive- and high-mass samples the average systematic uncertainty is approximately, $^{+12}_{-9}\%$ and $^{+10}_{-14}\%$, respectively. The equivalent values in the four-jet semi-inclusive- and high-mass samples are $^{+15}_{-15}\%$ and $^{+12}_{-17}\%$, respectively.

9 Results and discussion

9.1 The $\mathrm{d}\sigma/\mathrm{d}x_\gamma^{\rm obs}$ cross section

Figure 3 shows the $x_\gamma^{\rm obs}$ distribution in the three- and four-jet, semi-inclusive- and high-mass samples. Each distribution exhibits a peak at $x_\gamma^{\rm obs} \approx 0.9$. The low $x_\gamma^{\rm obs}$ region is kinematically suppressed. This low $x_\gamma^{\rm obs}$ suppression is more obvious in the high-mass samples. The ratio of the height of the high $x_\gamma^{\rm obs}$ peak divided by that of the low $x_\gamma^{\rm obs}$ peak, is smaller in the four-jet semi-inclusive-mass sample compared to the corresponding three-jet sample.

A comparison of the three-jet data with the MC predictions shows that those without MPIs are in good agreement with the high-mass cross section (Fig. 3b) but underestimate it at low $x_\gamma^{\rm obs}$, in the semi-inclusive-mass region (Fig. 3a). This is even more striking in the four-jet case.

In the low mass region, it is possible that MPIs augment the cross section. Figure 3 also contains the predictions from the MC models with MPIs included. The PYTHIA model, tuned to generic collider data, overestimates the three-jet semi-inclusive-mass cross section in the low $x_\gamma^{\rm obs}$ region, although describes it well in the highest two $x_\gamma^{\rm obs}$ bins (Fig. 3a). The same general behaviour is also seen in the four-jet case. In contrast, the HERWIG model with MPIs, which was tuned to the three- and four-jet $x_\gamma^{\rm obs}$ and M_{nj} data presented here, describes both the three- and four-jet data well in both mass regions.

The peak around $x_\gamma^{\rm obs} = 0.9$, in all four samples, is well described by the tuned HERWIG and is attributed in part to direct photoproduction events, which are solely found at high $x_\gamma^{\rm obs}$. The HERWIG model also predicts a significant contribution from resolved photoproduction even at high $x_\gamma^{\rm obs}$.

9.2 The $\mathrm{d}\sigma/\mathrm{d}M_{\rm nj}$ cross section

Figure 4 shows the three- and four-jet cross sections measured differentially in $M_{\rm nj}$. In general, both the three- and four-jet cross sections decrease exponentially with increasing $M_{\rm nj}$, although both deviate from this behaviour in the lowest mass region. This is due to a reduction in the available phase-space at low $M_{\rm nj}$ caused by the $E_T^{\rm jet}$ criteria.

Both the HERWIG and PYTHIA models predict that the fraction of resolved events and the presence of MPIs has a mass dependence. Included in Fig. 4 are the predictions of both HERWIG and PYTHIA without MPIs. Both MC models describe the $\mathrm{d}\sigma/\mathrm{d}M_{\rm nj}$ cross sections well at high $M_{\rm nj}$ but significantly underestimate them at lower values. In the three-jet case, the MC predictions are reasonable above $M_{\rm 3j} \approx 45$ GeV, whereas the four-jet cross section is described by the models for $M_{\rm 4j} \gtrsim 55$ GeV. This agreement suggests that MPIs do not contribute to the cross sections at masses above these values.

9.3 The $\mathrm{d}\sigma/\mathrm{d}y$ cross section

Figure 5 shows the y distribution in the three- and four-jet, semi-inclusive- and high-mass samples. The high-mass three-jet and both four-jet cross sections are observed to increase almost linearly with y, while that in the semi-inclusive-mass three-jet sample is approximately constant in y. The shape of the distributions is governed by the available kinematic phase-space, which shrinks with decreasing y, and the energy distribution of the photons within the incoming beam. This distribution is described by the Weizsäcker-Williams approximation [37]. The $\mathrm{d}\sigma/\mathrm{d}y$ cross sections are better described by HERWIG and PYTHIA, without MPIs. This suggests that the y dependence of MPIs may need to be revised.

9.4 Comparison of the three-jet results with $\mathcal{O}(\alpha\alpha_s^2)$ pQCD

The measured $M_{3\mathrm{j}}$ cross section is shown in Fig. 6 compared to that predicted by the $\mathcal{O}(\alpha\alpha_s^2)$ pQCD calculation, corrected for hadronisation effects and MPIs. The theoretical uncertainties are large, as is expected from a LO calculation. The calculation largely agrees with the measured cross section at high $M_{3\mathrm{j}}$ but underestimates the cross section at low $M_{3\mathrm{j}}$. This is seen in the ratio of the measured and predicted cross sections (lowest plot in Fig. 6). The hadronisation corrections are constant in $M_{3\mathrm{j}}$ but the MPI corrections increase significantly towards low $M_{3\mathrm{j}}$.

The comparison between the measured and calculated $\cos(\psi_3)$ cross sections is shown for the semi-inclusive- and high-mass samples in Figs. 7a and 7b, respectively. The ratio of the data divided by the predictions is also shown, as are the hadronisation and MPI corrections. The ratio in Fig. 7b shows that the calculation agrees with the measured cross section in the high-mass region. However, in the semi-inclusive-mass region (Fig. 7a) there is a difference between the measured and calculated cross sections. In particular, the measured cross section is larger as $|\cos(\psi_3)| \to 1$ than the $\mathcal{O}(\alpha\alpha_s^2)$ theory predicts. In this case, however, the shape difference is less likely due to an underestimation of the MPI or hadronisation corrections since they are both largely independent of $\cos(\psi_3)$.

10 Summary

Three- and four-jet states have been measured in γp collisions at HERA, using an integrated luminosity of 121 pb^{-1}. Both the three- and four-jet events have been studied in a semi-inclusive, $M_{\mathrm{nj}} \geq 25$ GeV, and high-mass region, $M_{\mathrm{nj}} \geq 50$ GeV. The three-jets have been measure with over seven times the luminosity of the previous HERA publication and a four-jet measurement in photoproduction has been attempted for the first time. The three-jet and four-jet cross sections are reasonably described by both PYTHIA and HERWIG, run without MPIs, in the high-mass region. In the semi-inclusive-mass region, the MC without MPIs underestimated the data. When MPIs were added to the MC simulations, the agreement between the models and data was generally improved, although the PYTHIA model, tuned to generic collider data, augmented the cross section too much.

The $\mathcal{O}(\alpha\alpha_s^2)$ pQCD calculation described the three-jet data for $M_{3\mathrm{j}} \gtrsim 50$ GeV. At lower masses the calculation gave a poorer description.

References

[1] ZEUS Coll., J. Breitweg et al., Phys. Lett. **B443**, 394 (1998).

[2] H1 Coll., I. Abt et al., Z. Phys. **C61**, 59 (1994).

[3] H1 Coll., C. Adloff et al., Phys. Lett. **B515**, 17 (2001).

[4] ZEUS Coll., S. Chekanov et al., hep-ex/0502007 (2005).

[5] ZEUS Coll., S. Chekanov et al., Phys. Lett. **B516**, 273 (2002).

[6] ZEUS Coll., M. Derrick et al., Phys. Lett. **B 297**, 404 (1992).

[7] ZEUS Coll., U. Holm (ed.), *The ZEUS Detector*. Status Report (unpublished), DESY (1993), available on `http://www-zeus.desy.de/bluebook/bluebook.html`.

[8] ZEUS Coll., J. Breitweg et al., Eur. Phys. J. **C 1**, 109 (1998).

[9] ZEUS Coll., J. Brietweg et al., Eur. Phys. J. **C6**, 43 (1999).

[10] G.M. Briskin, *Diffractive Dissociation in ep Deep Inelastic Scattering*. Ph.D. Thesis, Tel Aviv University, Tel Aviv, Israel, 1998.

[11] ZEUS Coll., J. Brietweg et al., Eur. Phys. J. **C11**, 35 (1999).

[12] S. Catani, Yu.L. Dokshitzer, M.H. Seymour and B.R. Webber, Nucl. Phys. **B406**, 187 (1993).

[13] S.D. Ellis and D.E. Soper, Phys. Rev. **D48**, 3160 (1993).

[14] G. Corcella, I.G. Knowles, G. Marchesini, S. Moretti, K. Odagiri, P. Richardson, M.H. Seymour and B.R. Webber, *HERWIG 6.5 Manual*, 2000, available on `http://hepwww.rl.ac.uk/theory/seymour/herwig/`;
G. Corcella, I.G. Knowles, G. Marchesini, S. Moretti, K. Odagiri, P. Richardson, M.H. Seymour and B.R. Webber, *HERWIG 6.5 Release Note*, 2001, available on `http://hepwww.rl.ac.uk/theory/seymour/herwig/`;
G. Marchesini, B.R. Webber, G. Abbiendi, I.G. Knowles, M.H. Seymour and L. Stanco, Computer Phys. Commun. **67**, 465 (1992).

[15] T. Sjöstrand, P. Edén, C. Friberg, L. Lönnblad, G. Miu, S. Mrenna and E. Norrbin, *PYTHIA 6.206 Manual*, 2002, available on `http://www.thep.lu.se/∼torbjorn/Pythia.html`;
T. Sjöstrand, P. Edén, C. Friberg, L. Lönnblad, G. Miu, S. Mrenna and E. Norrbin, Computer Phys. Commun. **135**, 238 (2001).

[16] G. Marchesini and B.R. Webber, Nucl. Phys. **B310**, 461 (1988).

[17] I.G. Knowles, Nucl. Phys. **B310**, 571 (1988).

[18] I.G. Knowles, Computer Phys. Commun. **58**, 271 (1990).

[19] B.R. Webber, Nucl. Phys **B238**, 492 (1984).

[20] B. Andersson, G. Gustafson, G. Ingelman and T. Sjöstrand, Phys. Rep. **97**, 31 (1983).

[21] T. Sjöstrand, Phys. Lett. **B142**, 420 (1984).

[22] J.M. Butterworth, J.R. Forshaw and M.H. Seymour, Z. Phys. **C72**, 637 (1996).

[23] J.M. Butterworth and J.R. Forshaw, J. Phys. **G19**, 1657 (1993).

[24] J.M. Butterworth, J.R. Forshaw, T. Sjöstrand and J.K. Storrow, J. Phys. **G22**, 883 (1996).

[25] J.M. Butterworth and M.H. Seymour, *JIMMY4: Multiparton Interactions in HERWIG for the LHC* (unpublished), 2005, available on `http://hepforge.cedar.ac.uk/jimmy/`.

[26] R. Brun, F. Bruyant, M. Maire, A. C. McPherson and P. Zanarini, *Geant3* (unpublished). CERN-DD/EE/84-1, 1987.

[27] CTEQ Coll., H.L. Lai et al., Eur. Phys. J. **C12**, 375 (2000).

[28] M. Gluck, E. Reya and A. Vogt, Z. Phys. **C53**, 127 (1992).

[29] T. Namsoo, *Three- and Four-Jet States in Photoproduction at HERA*. Ph.D. Thesis, University of Bristol, Bristol, UK, 2006.

[30] M. Gluck, E. Reya and A. Vogt, Z. Phys. **C67**, 433 (1995).

[31] K. Hagiwara, M. Tanaka, I. Watanabe and T. Izubuchi, Phys. Rev. **D51**, 3197 (1995).

[32] C. Gwenlan, *Jets and Energy Flow in Photoproduction using the ZEUS Detector at HERA*. Ph.D. Thesis, UCL, London, UK, 2003.

[33] M. Klasen, T. Kleinwort and G. Kramer, Z. Phys. Rev.-e **C1** (1998).

[34] M. Klasen, hep-ph/9808223.

[35] CTEQ Coll., H.L. Lai et al., Phys. Rev. **D55**, 1280 (1997).

[36] M. Gluck, E. Reya and A. Vogt, Phys. Rev. **D45**, 3986 (1992).

[37] C.F. von Weizsäcker, Z. Phys. **88**, 612 (1934);
E.J. Williams, Phys. Rev. **45**, 729 (1934);
S. Frixione, M.L. Mangano, P. Nason and G. Ridolfi, Phys. Lett. **B319**, 339 (1993).

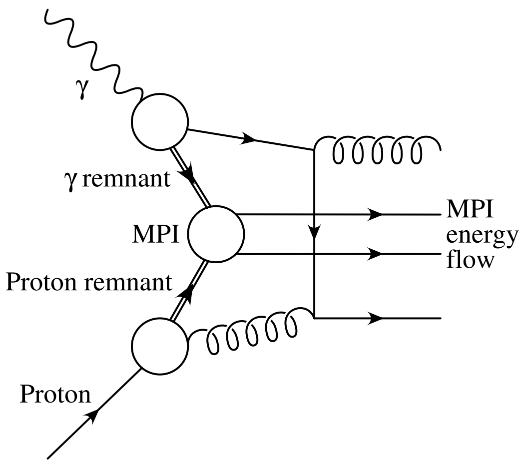

Figure 1: *A multi-parton interaction occurring in a resolved photoproduction event. As well as a hard primary interaction occurring between the proton and the hadron-like photon, a secondary interaction occurs between the proton and photon remnants leading to additional energy flow in the final state.*

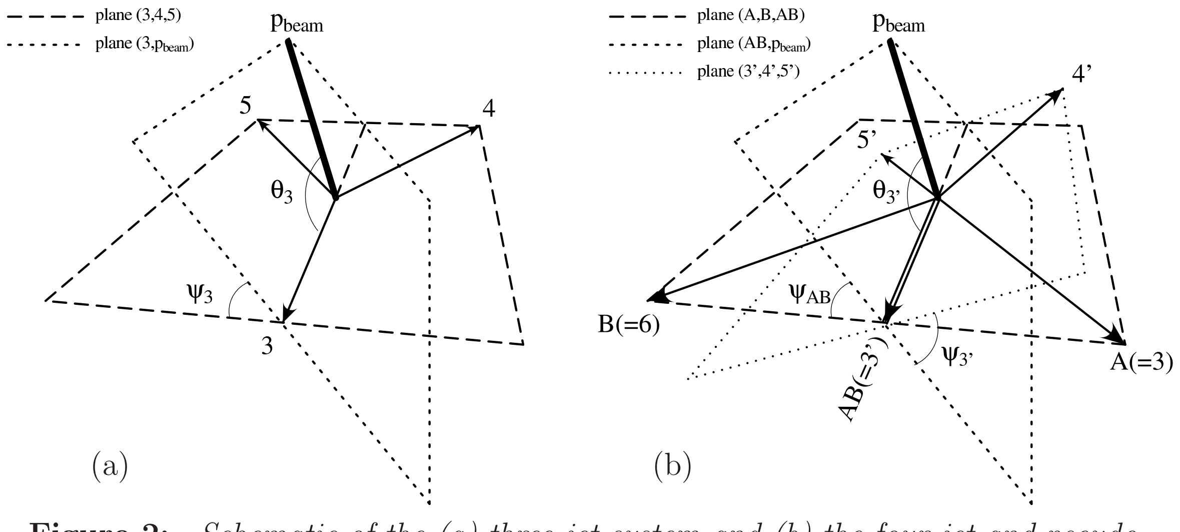

Figure 2: *Schematic of the (a) three-jet system and (b) the four-jet and pseudo-three-jet system and the various angles that are conventionally used to span the kinematic space of either multi-jet system.*

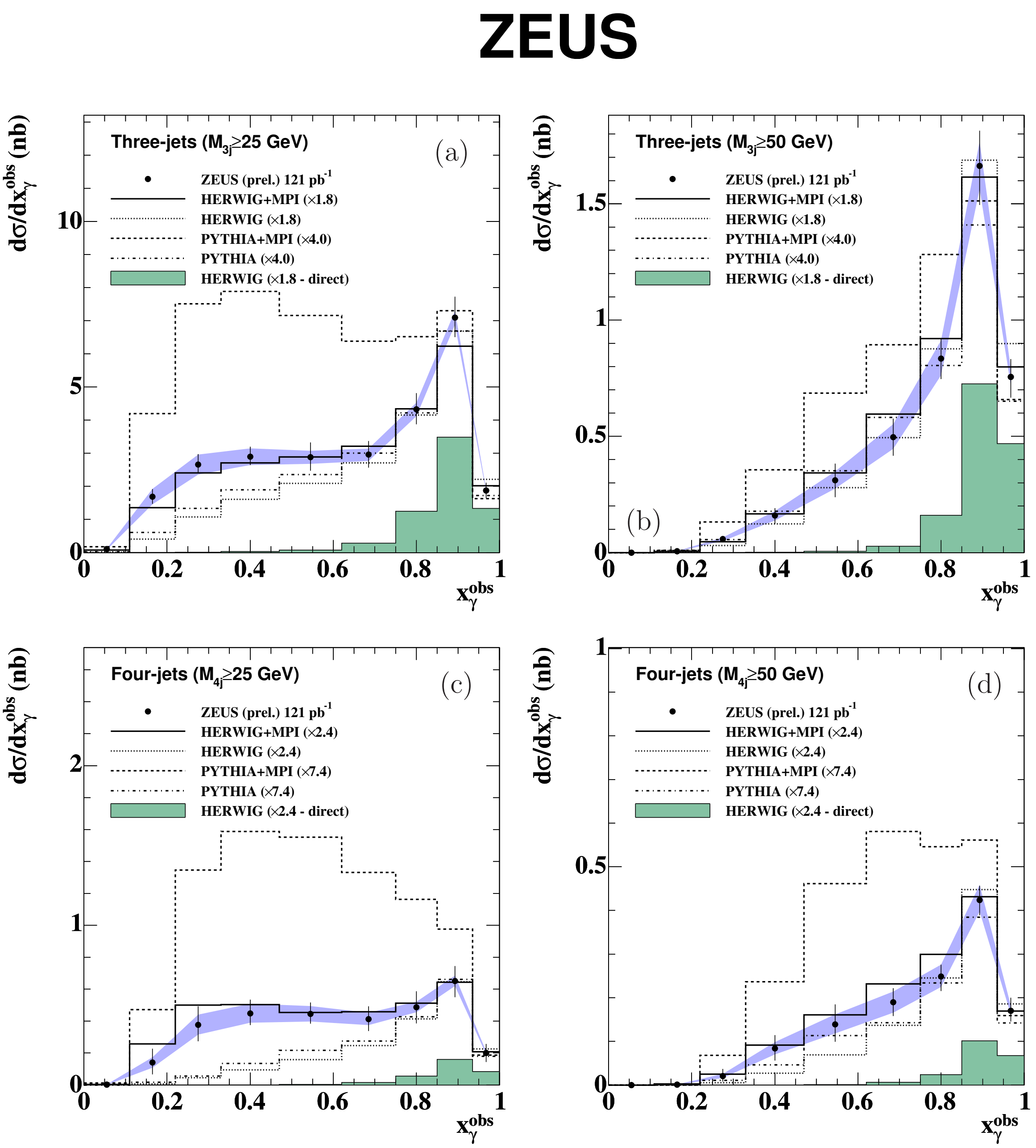

Figure 3: *The x_γ^{obs} cross section in the three-jet, semi-inclusive- (a) and high-mass (b) regions and the four-jet, semi-inclusive- (c) and high-mass (d) regions. The calorimeter energy scale uncertainty is represented by the shaded band. Shown also are the* Herwig *and* Pythia *predictions, with and without MPIs, as well as the* Herwig *direct component. Each Monte Carlo cross section has been scaled by the amount indicated in the legend.*

ZEUS-prel-06-009

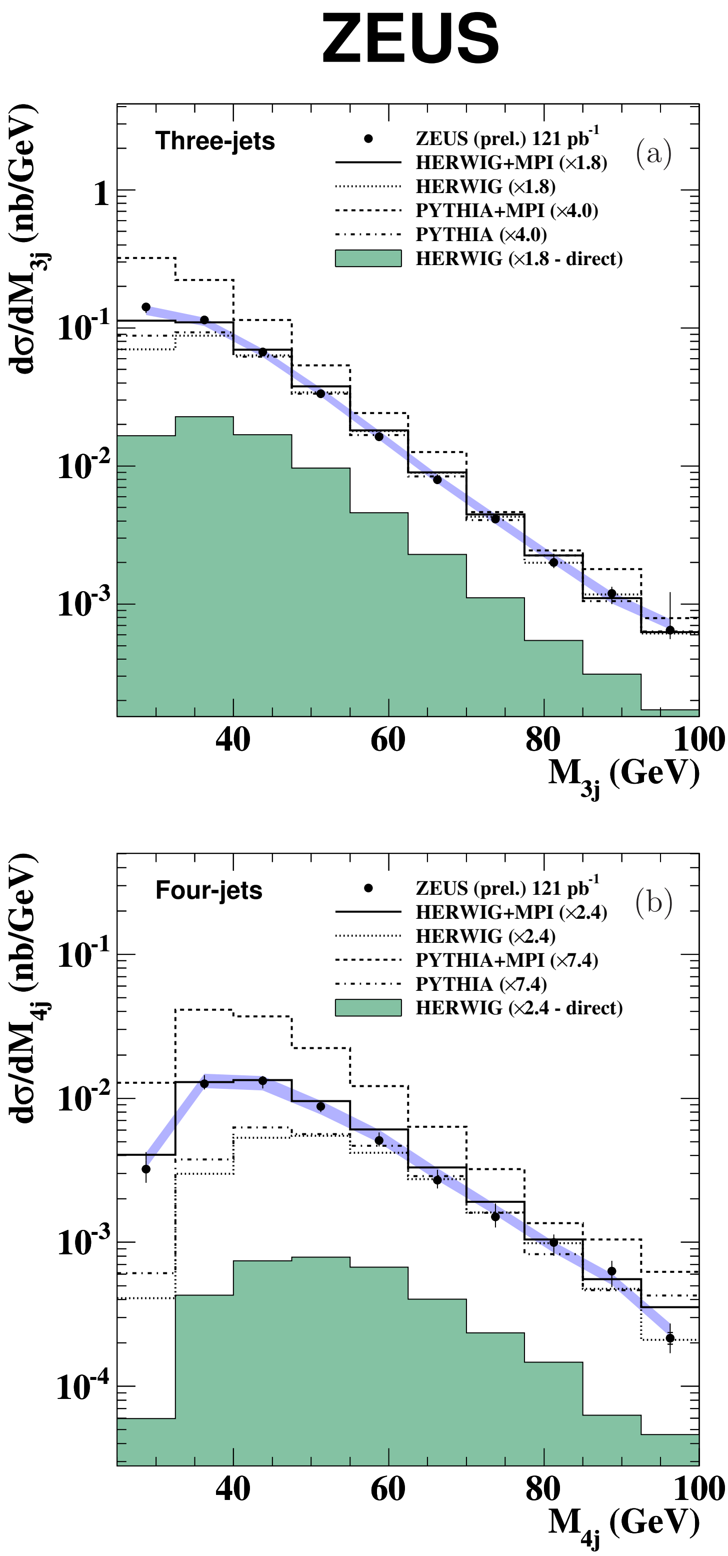

Figure 4: *The M_{3j} cross section in the semi-inclusive-mass, three-jet sample (a) and the M_{4j} cross section in the semi-inclusive-mass, four-jet sample (b). The calorimeter energy scale uncertainty is represented by the shaded band. Shown also are the* Herwig *and* Pythia *predictions, with and without MPIs, as well as the* Herwig *direct component. Each Monte Carlo cross section has been scaled by the amount indicated in the legend.*

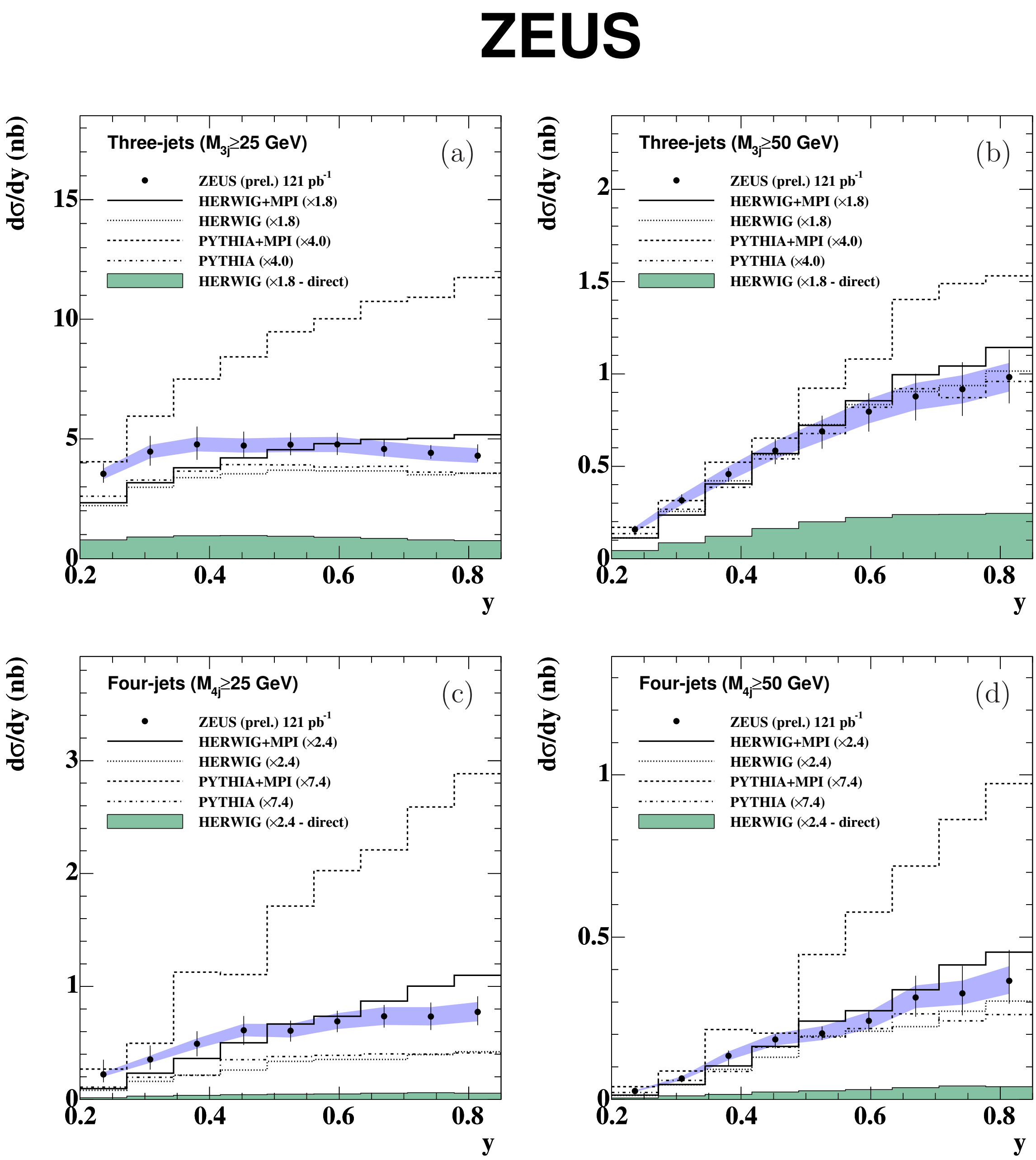

Figure 5: *The y cross section in the three-jet, semi-inclusive- (a) and high-mass (b) regions and the four-jet, semi-inclusive- (c) and high-mass (d) regions. The calorimeter energy scale uncertainty is represented by the shaded band. Shown also are the* Herwig *and* Pythia *predictions, with and without MPIs, as well as the* Herwig *direct component. Each Monte Carlo cross section has been scaled by the amount indicated in the legend.*

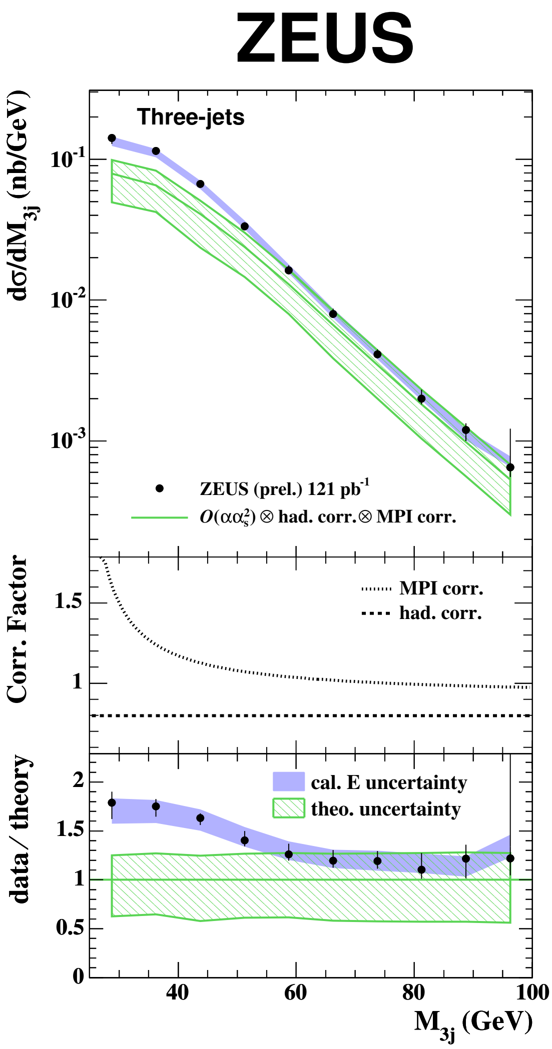

Figure 6: *The M_{3j} cross section in the three-jet sample compared with the $\mathcal{O}(\alpha\alpha_s^2)$ pQCD prediction, which has been convoluted with both hadronisation and MPI corrections. The bin-by-bin hadronisation and MPI corrections are given. The ratio of the M_{3j} cross section divided by the convoluted $\mathcal{O}(\alpha\alpha_s^2)$ prediction is also shown. The calorimeter energy scale uncertainty and theoretical scale uncertainty are represented by shaded bands.*

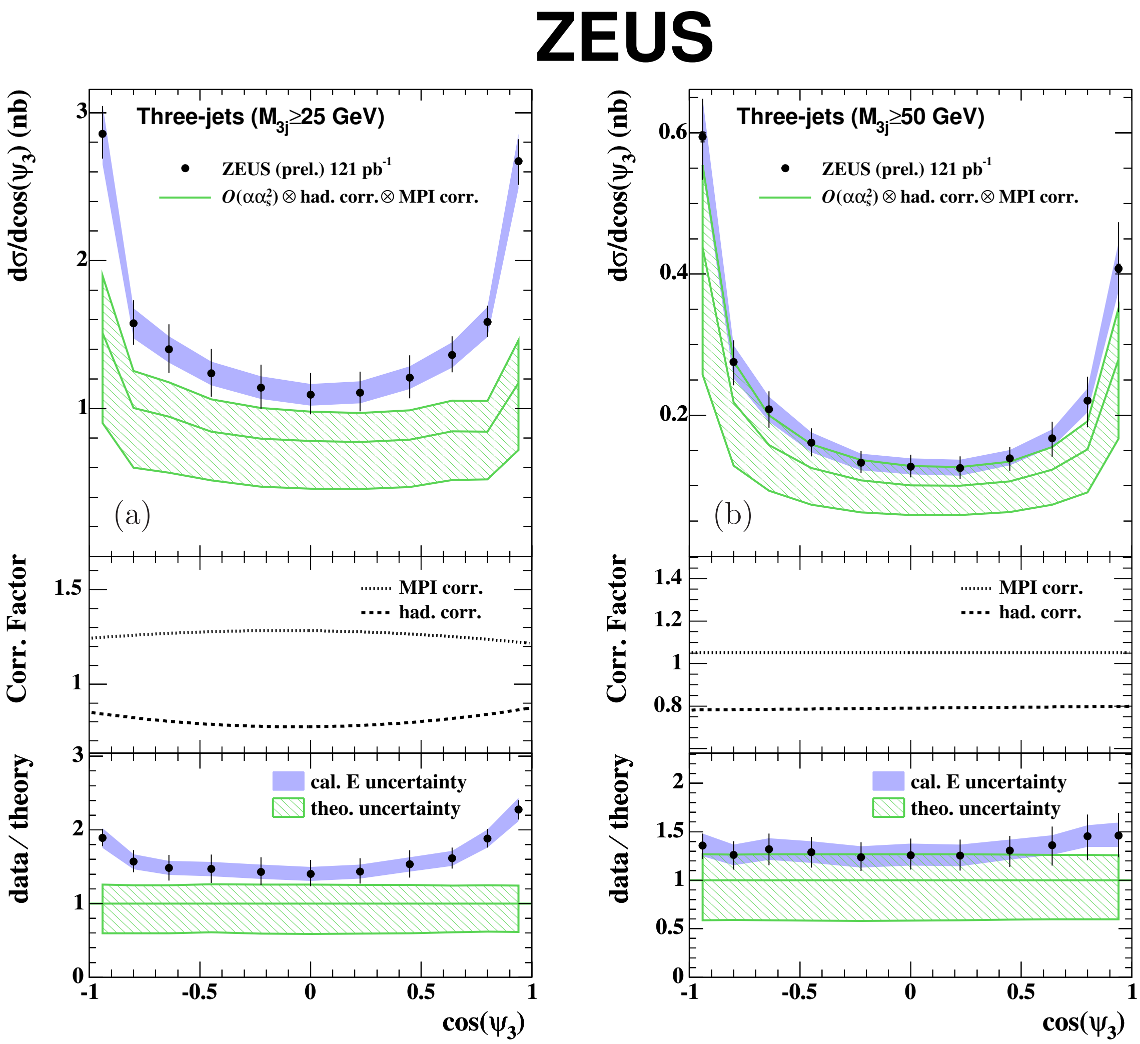

Figure 7: *The* $\cos(\psi_3)$ *cross sections in the semi-inclusive- (a) and high-mass (b), three-jet samples compared with the* $\mathcal{O}(\alpha\alpha_s^2)$ *pQCD predictions, which have been convoluted with both hadronisation and MPI corrections. The bin-by-bin hadronisation and MPI corrections are given. The ratio of the* $\cos(\psi_3)$ *cross sections divided by the convoluted* $\mathcal{O}(\alpha\alpha_s^2)$ *predictions are also shown. The calorimeter energy scale uncertainty and theoretical scale uncertainty are represented by shaded bands.*